

# A Self-Supervised Approach for Cluster Assessment of High-Dimensional Data

Alokendu Mazumder<sup>1</sup>, Pagadala Krishna Murthy<sup>1</sup>, and Punit Rathore<sup>1</sup>

<sup>1</sup>Robert Bosch Centre for Cyber-Physical Systems, Indian Institute of Science Bangalore, Bengaluru, India

<sup>1</sup>Email ID:{alokendum, pagadalam, prathore}@iisc.ac.in

**Abstract**—Estimating the number of clusters and underlying cluster structure in a dataset is a crucial task. Real-world data are often unlabeled, complex and high-dimensional, which makes it difficult for traditional clustering algorithms to perform well. In recent years, a matrix reordering based algorithm, called *visual assessment of tendency* (VAT), and its variants have attracted many researchers from various domains to estimate the number of clusters and inherent cluster structure present in the data. However, these algorithms fail when applied to high-dimensional data due to the curse of dimensionality, as they rely heavily on the notions of *closeness* and *farness* between data points. To address this issue, we propose a deep-learning based framework for cluster structure assessment in complex, image datasets. First, our framework generates representative embeddings for complex data using a self-supervised deep neural network, and then, these low-dimensional embeddings are fed to VAT/iVAT algorithms to estimate the underlying cluster structure. In this process, we ensured not to use any prior knowledge for the number of clusters (i.e.  $k$ ). We present our results on four real-life image datasets, and our findings indicate that our framework outperforms state-of-the-art VAT/iVAT algorithms in terms of clustering accuracy and normalized mutual information (NMI).

**Index Terms**—Visual assessment of tendency, cluster structure, self-supervised network.

## I. INTRODUCTION

Data clustering is a widely used unsupervised learning technique that involves dividing a collection of unlabeled objects into  $k$  groups of similar objects. There are various clustering algorithms available in the literature, such as hierarchical clustering, centroid-based approaches, density-based algorithms, and distribution-based clustering. Most clustering algorithms require  $k$ , the number of clusters to seek, as an input, which is the clustering tendency assessment problem. One common method to determine the number of clusters and their underlying structure is to visualize the data points using a 2D or 3D plot. However, this approach is only feasible for two- or three-dimensional datasets. For high-dimensional datasets such as images, time-series, visualizing and interpreting cluster structures using 2D or 3D visualization is not practical. Although various dimensionality reduction techniques, such as principal component analysis (PCA) and linear discriminant analysis (LDA), exist in the literature, these techniques often result in a low-dimensional representation of complex, high-dimensional datasets that may not fully reflect the inherent cluster structure due to information loss.

There are various formal (based on statistics) and informal (other approaches) techniques [1], [2] available in the

literature for cluster structure assessment, but they are not completely effective. In contrast, visual approaches [3] have been in use for many years and serve as the foundation for many visual data analysis methods. The *Visual Assessment of Clustering Tendency* (VAT) [4], a matrix reordering-based visual-analytical method, is one of such algorithm which provides a visual way to assess the clustering tendency of various datasets. There are several variants of VAT available for different types of data, which are collectively known as the VAT family of algorithms. The VAT family of algorithms has become an acceptable and widely used tool in several domains like biomedical applications, speech processing, image segmentation, transportation applications, and *etc* for exploratory data analysis.

VAT algorithm employs a variant of Prim’s minimum spanning tree algorithm [5] to perform matrix reordering of the pairwise dissimilarity matrix to generate a reordered dissimilarity matrix. The reordered dissimilarity matrix can be viewed as a monochrome image called a *Reordered Dissimilarity Image* (RDI) or cluster heat map. The RDI displays a possible cluster structure of the data set by showing dark blocks along the diagonal. One method to obtain an accurate estimate of the number of clusters ( $k$ ) from the RDI in the data is to count the number of dark blocks along the diagonal of the RDI.

This method is particularly effective for datasets with well-separated, compact clusters since the dark blocks along the diagonal are easily identifiable. However, for complex datasets (e.g., images, time-series) having overlapping cluster structures (which is the case for most real-life datasets), existing VAT approaches perform poorly as the RDI quality degrades and the contrast between dark blocks along the diagonal and the rest of the image decrease. This makes it difficult to count the dark blocks along the diagonal.

There have been some efforts [6]–[8] to improve the quality of VAT generated RDI to accurately estimate the number of clusters for various complex geometry datasets. However, these algorithms perform poorly on image datasets, particularly those having overlapping clusters. Typically, images are flattened prior to the application of clustering algorithms, including those in the VAT family, resulting in high-dimensional data. Hence, the pixel-wise Euclidean distance becomes less effective in capturing similarities or dissimilarities between images, due to the curse of dimensionality. Fig. 1 shows an iVAT RDI for a synthetic, high-dimensional dataset (number of

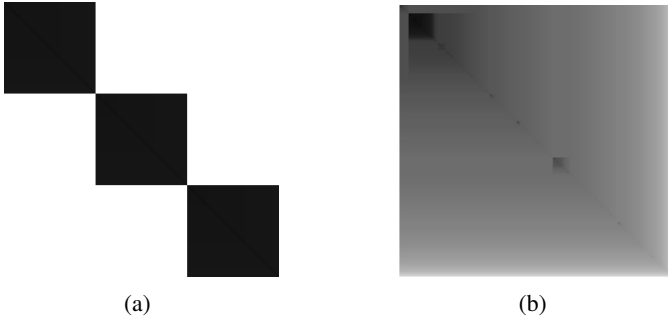


Fig. 1: (a) iVAT image of 100-dimensional Gaussian mixture data (3 Gaussians); (b) iVAT image of flattened MNIST data (784 dimensional)

samples = 1000, dimensions= 100) having three well-separated Gaussian mixtures (so  $k=3$ ) in View (a), and RDI for a sample of popular MNIST dataset (number of samples = 1000 dimensions= 784,  $k = 10$  classes) in View (b). It is evident from the figure that iVAT performs well when the data has inherently well separated clusters as we can clearly see three dark blocks along the diagonal in its RDI representing three clusters. However, it fails miserably for very high-dimensional, image dataset like MNIST as we can not see any clear dark blocks in its RDI.

To remedy these concerns, we propose a deep learning based visual-analytical framework, DeepVAT, for cluster structure assessment to discover deep cluster structures present in high-dimensional data, when no ground truths are available, i.e., data is unlabeled. Our major contributions are as follows:

- We proposed a deep, self-supervised learning framework, DeepVAT, that can provide visual evidence of the number of clusters present in complex, high-dimensional data.
- We performed experiments on four real-world, publicly available, large image datasets to show the superiority of DeepVAT over other state-of-the-art VAT family algorithms (proposed for high-dimensional data) in terms of image quality, clustering accuracy, and normalized mutual information (NMI) score.

To our knowledge, this is the first work in the literature investigating the effects of deep features for VAT methods.

Here is an outline of the rest of this article. Section II presents the preliminaries for the VAT/iVAT algorithm and reviews related work. The proposed algorithm, DeepVAT, is discussed in Section III. Section IV discusses the experiments and results, followed by conclusions in Section V.

## II. PRELIMINARIES AND RELATED WORK

### A. VAT, iVAT, and SpecVAT

Consider we have a set of  $N$  objects, denoted as  $O = o_1, o_2, \dots, o_N$ , where each object in  $O$  is described by a  $p$ -dimensional feature vector ( $\in \mathbb{R}^p$ ). Alternatively, the data can be represented as a dissimilarity matrix, denoted as  $D_N = [d_{ij}]$ , where  $d_{ij}$  indicates the dissimilarity between object  $o_i$  and object  $o_j$  computed using a suitable distance measure. The

VAT algorithm considers the dissimilarity matrix,  $D_N$  as an input and reorders (by shuffling the rows and columns) using a modified Prim's algorithm. The image  $I(D_N)$  of the reordered distance matrix  $D_N$  displays each pixel's intensity to indicate the dissimilarity between the corresponding row and column objects. When dark blocks appear along the diagonal, they might represent distinct clusters, ideally  $k$  clusters. As single-linkage clusters are always diagonally aligned in VAT ordered images [9],  $k$  aligned clusters can be obtained by cutting the largest  $(k - 1)$  edges (given by the MST cut magnitude order  $d$ ) from the MST.

The improved-VAT (iVAT) [6] enhances the quality of VAT [4] RDI by using path-based distance transformation. The iVAT transformed matrix  $D'_N = [d'_{ij}]$  is generated using a path-based minimax distance [5]:

$$d'_{ij} = \min_{p \in P_{ij}} \max_{1 < h < |r|} \mathbf{D}_{p[h]p[h+1]} \quad (1)$$

where  $p \in P_{ij}$  is an acyclic path in the set of all acyclic paths between objects  $(o_i)$  and  $(o_j)$  (vertices  $i$  and  $j$ ) in  $O$ .

The SpecVAT [10] algorithm is another approach that improves the quality of the RDI produced by VAT. It utilizes spectral graph theory to transform the raw distance matrix into a graph embedding space using graph Laplacian. It then creates an alternative feature representation of the data by selecting the  $k$  most significant eigenvectors that correspond to the highest eigenvalues. VAT is then applied to this transformed representation, resulting in a much-improved RDI.

### B. VAT Variants for Large Volumes of High-Dimensional Data

Although the VAT tool, discussed above, find its usefulness in many applications, they can be computationally expensive as the size of the data set grows due to its  $\mathcal{O}(N^2)$  complexity. To understand the clustering structure for large volume datasets, a scalable version of VAT called *scalable VAT* (sVAT) was developed by Hathaway *et al.* [11], which utilizes a smart sampling based approach. To begin, sVAT extracts a smart sample of size  $n$  (where  $n \ll N$ ) from the large data set  $X$  using maximin random sampling (MMRS) [12]. The extracted sample is then used to compute the distance matrix  $D_n$ , which is input into VAT.

To handle large volumes of high-dimensional datasets, our previous work introduced FensiVAT [7], an ensemble-based, hybrid clustering framework that combines fast data-space reduction with an intelligent sampling strategy to assess the clustering tendency of high-dimensional data. Recently, Zhang *et al.* [8] proposed another method that leverages a kernel-based dissimilarity matrix to refine the RDI further, called kernel-based iVAT (KernelVAT). They use a Gaussian kernel and isolation kernel (data-dependent) to transform the RDI.

To our knowledge, none of the existing VAT family of algorithms, including those reviewed in this section, have been investigated thoroughly on image datasets. Moreover, they have shown to perform poorly on image datasets in their numerical experiments. Below, we discuss our proposed framework, DeepVAT.

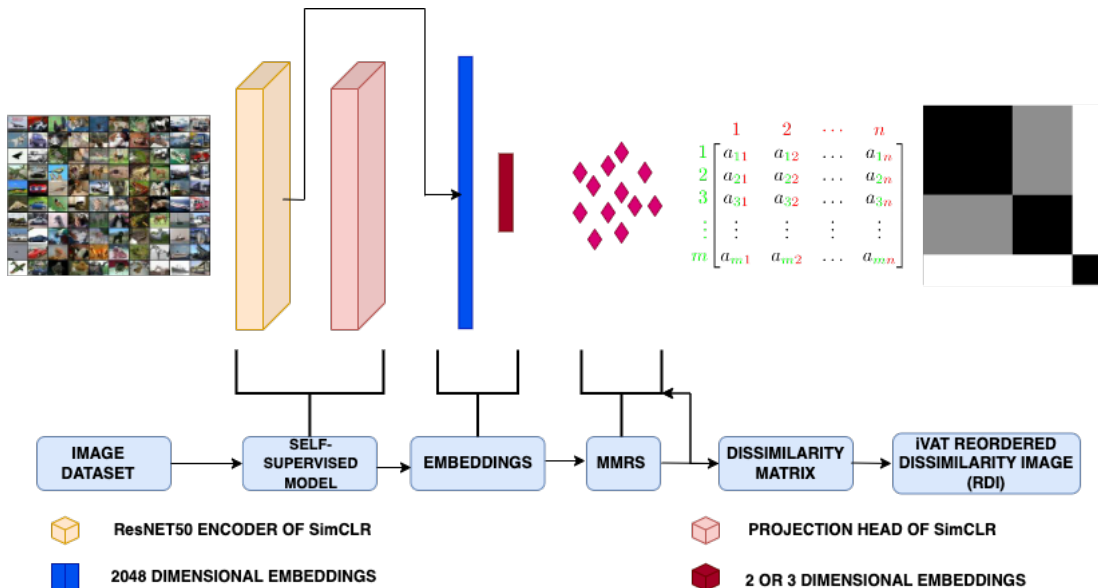


Fig. 2: The proposed architecture of DeepVAT

### III. PROPOSED FRAMEWORK: DEEPVAT

In this paper, we propose a deep learning-based framework, DeepVAT, to advance VAT family of algorithms for cluster structure assessment in complex, high-dimensional image datasets. Fig. 2 presents each step of our proposed framework. Below, we briefly explain each step of DeepVAT keyed to the blocks shown in Fig. 2.

#### A. Generating Image Embeddings

The first step in our framework is representation learning by employing deep learning architectures. Recently, a wide range of self-supervised approaches such as contrastive learning based models have been proposed that can provide clustering-friendly representations for images using deep neural networks, without the need for ground truth information. These models include *Simple Contrastive Learning of Representations* (SimCLR) [13], Barlow Twins [14], *Decoupled Contrastive Learning* (DCL) [15], SimSiam [16], *Bootstrap Your Own Latent* (BYOL) [17], and many others. The goal of this step is to ensure that similar data points are brought closer to each other, while dissimilar points are pushed further away.

During our research, we conducted experiments with embeddings generated by some of these models for VAT algorithm, and we found that embeddings generated by SimCLR produced iVAT images were considerably superior to those generated by other contrastive-learning models. We also noticed that the training time for SimCLR was significantly lesser than other models. Consequently, we chose SimCLR as our primary model for creating embeddings in our proposed framework.

In SimCLR, the first stage includes performing auxiliary tasks on a given batch of images, such as corrupting the data, adding noise, and creating augmented views of the same data. These transformations generate fresh views of the

same images, effectively enlarging the training set. Gray-scale images cannot undergo certain transformations such as color jitters. Instead, an affine stretch is utilized along with rotation, resizing, and blurring. Through these tasks, the models can acquire a rich and beneficial representation of the data.

SimCLR consists of an encoder network and a non-linear projection head. The augmented images are fed into the encoder to extract high-level features. The encoder consists of several convolutional and fully connected layers and is trained using a contrastive loss function. The SimCLR framework utilizes an InfoNCE loss function [18] to measure the similarity between different views of an image. The model aims to maximize the similarity between the two views of the same image and minimize the similarity between views of different images. By doing so, SimCLR learns to extract valuable features robust to variations in the input data, which is helpful for generalization in real-world scenarios. The encoder projects the images into (say)  $d$ -dimensional space.

Then, the projection head, a small neural network, further maps the encoded features ( $d$ -dimensional) to a (lower)  $m$ -dimensional set of embeddings, and then back to a lower-manifold of  $d$ -dimensional space, resulting in a rank-deficient weight matrix. This projection head is trained alongside the encoder during training. After training successfully, the projection head is discarded, and the data is passed through the trained encoder to generate embeddings. The projection head serves as an additional non-linear transformation that helps to increase the quality of the learned features.

#### B. Dimensional Reduction using $t$ -SNE

Despite the fact that SimCLR embeddings (shown with blue vertical bar in Fig. 2) can be used to compute the dissimilarity matrix for VAT/iVAT, the high dimensionality of the SimCLR embeddings can lead to the curse of dimensionality problem,

which can affect the quality of the resulting visualization. In our experiments, as discussed in Section IV, we observed that using SimCLR embeddings to compute the dissimilarity matrix did not result in a significant improvement in the quality of the resulting RDI images.

One way to tackle this issue is to apply t-SNE on a data representation obtained from SimCLR. Compared to the original input data, t-SNE works better on SimCLR embeddings because SimCLR is a deep-layer architecture that can more efficiently represent the highly varying data manifold in multiple nonlinear layers [13], [19]. The projections generated by SimCLR’s projection head can identify highly varying manifolds better than a local method like t-SNE, resulting in a higher quality visualization compared to using t-SNE on the original high-dimensional data.

### C. Smart Sampling: Maximin Random Sampling (MMRS)

Computing and analyzing VAT RDI using t-SNE embeddings (shown with red vertical bar in Fig. 2), generated in the last step, may be infeasible for large image datasets (large  $N$ ) due to  $\mathcal{O}(N^2)$  complexity of VAT. To deal with large image datasets, we exploit a smart sampling approach called *Maximin and Random Sampling* (MMRS) which was introduced in our previous work [7].

Let  $\mathbf{X} = \{x_i\}_{i=1}^N$  be the set of embeddings generated from the trained encoder and applying t-SNE on them, where  $x_i \in \mathbb{R}^2$  or  $\mathbb{R}^3$ . The MMRS technique is an intelligent way to obtain samples in large batch data sets by combining maximin (MM) and random sampling (RS). The MM sampling process starts by identifying a set of  $k'$  (an overestimate of  $k$ ) distinguished objects, which are the farthest from each other in the input data  $X$ . Then each point in the set  $X$  is grouped with its nearest distinguished object using the nearest prototype rule (NPR), which divides the entire dataset into  $k'$  groups  $\{G_i\}_{i=1}^{k'}$  where  $G_i \subseteq X$ ,  $\forall i \in \{1, 2, \dots, k'\}$  by associating  $|G_i|$  points to  $i^{\text{th}}$  MM sample, which represents each of the  $k'$  group. Finally, the sample  $\mathcal{S}$  of size  $n \ll N$  is formed by selecting random data-points from each of the  $k'$  groups  $\{G_i\}_{i=1}^{k'}$ . The number of points  $n_j$  extracted from group  $G_j$  is proportional to the cardinality of  $G_j$ , i.e  $n_j \propto |G_j|$ . To be precise,  $n_j = \lceil n \times |G_j| / N \rceil$ , where  $\lceil \cdot \rceil$  is the ceiling function. This step gives us a smart sample of size  $n \ll N$  in lower dimensional space. Rather than feeding a large number of embeddings directly into iVAT for visualization, we feed a *smart sample* of size  $n$ , obtained using MMRS.

### D. Dissimilarity Matrix Computation for VAT/iVAT

The reduced-dimension, smart samples are used to compute dissimilarity matrix  $D_n$  which is fed to the VAT/iVAT algorithm to obtain reordered dissimilarity matrix  $D'_n$ . The visualization of  $I(D'_n)$  suggests the number of clusters  $k$  present in the dataset.

## IV. EXPERIMENTS

We performed experiments on four publicly available, real, image datasets. We evaluated the ability of DeepVAT to suggest the number of clusters in image datasets, and compared

its performance with iVAT and other VAT family methods that are claimed to work better with high-dimensional data.

### A. Datasets

We performed our experiments on the following datasets:

- **MNIST** [20]: It has a total of 60,000 grayscale images of digits with a dimension of  $28 * 28$  ranging from 0 to 9, i.e., total 10 classes, with each class having 6,000 images. We randomly sampled 3,000 images from each class and experimented on 30,000 images.
- **FMNIST** [21]: It has total of 60,000 grayscale images of fashion apparel with a dimension of  $28 * 28$ , i.e., it has total 10 classes, with each class having 6,000 images. We randomly sampled 3,000 images from each class.
- **CIFAR10** [22]: It has a total of 50,000 natural RGB images with a dimension of  $32 * 32 * 3$ . It has total 10 classes, with each class having 5,000 images. We randomly sampled 3000 images from each class.
- **Intel Image Dataset** [23]: It has 14,034 natural RGB training images and 3,000 testing images with 6 classes. We clubbed both sets and used the final count of 17,000 images to perform various experiments. Each image has a dimension of  $32 * 32 * 3$ .

### B. Parameter Settings

The SimCLR model was trained using the LARS optimizer [24] for each dataset, with 1,000 epochs. The output dimension of the encoder network was set to  $d = 2,048$ , and the projection head network was chosen to have  $m = 128$ . The experiments were conducted on a regular PC with the following configuration: OS: Ubuntu 22.04.2 LTS (64 bit); processor: Intel(R) Xeon(R) Gold 5220R CPU @ 2.20GHz; RAM: 62 GB; GPU: Nvidia Quadro RTX 6000, 24 GB. We performed each experiment five times on each dataset and reported the average results. We use a batch size of 700 for MNIST and FMNIST and 256 for CIFAR10 and Intel Image Dataset. The parameters for MMRS sampling are:  $k' = 15$  for MNIST, FMNIST, and CIFAR10, and 10 for INTEL, number of samples,  $n$ : 4,000 for all datasets.

### C. Evaluation Criteria

We show all (best) iVAT images with estimated number of clusters  $k_p$  for all the compared algorithms for qualitative analysis. We also evaluate the quantitative performance in terms of partition accuracy (PA) for the estimated value of  $k$  (from iVAT image) and normalized mutual information (NMI) using ground truth information for each dataset. The PA of a clustering algorithm is the % ratio of the number of samples with matching ground truth and algorithmic labels to the total number of samples in the dataset. A higher value of PA and NMI implies a better match to the ground truth partition.

### D. Comparison of DeepVAT with other VAT families

In this section, we make quantitative and qualitative comparisons of DeepVAT with simple iVAT and existing VAT family methods that claim to work better with high dimensional data,


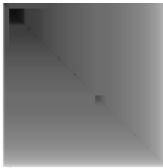


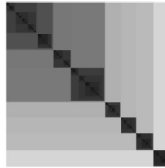
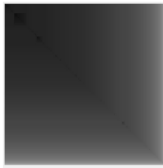

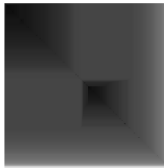

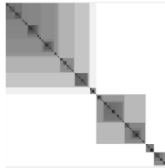

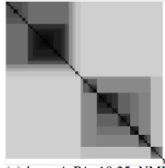
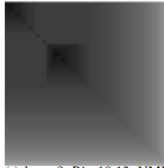

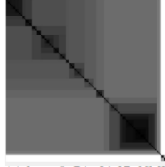

Dataset	Methods Used						
	DeepVAT	$I(\mathbf{D}_V)$	$I(\mathbf{D}_{V-t-SNE})$	$I(\mathbf{D}_F)$	$I(\mathbf{D}_{F-t-SNE})$	$I(\mathbf{D}_K)$	$I(\mathbf{D}_{K-t-SNE})$
MNIST	 (a) $k_p = 9$ , PA: 86.95, NMI: 0.90	 (b) $k_p = 1$ , PA: 10.05, NMI: 0.01	 (c) $k_p = 8$ , PA: 39.94, NMI: 0.57	 (d) $k_p = 2$ , PA: 10.01, NMI: 0.016	 (e) $k_p = 7$ , PA: 39.63, NMI: 61.42	 (f) $k_p = 1$ , PA: 13.21, NMI: 0.017	 (g) $k_p = 8$ , PA: 39.04, NMI: 0.57
( $k = 10$ ) FMNIST	 (h) $k_p = 7$ , PA: 50.00, NMI: 0.66	 (i) $k_p = 0$ , PA: 10.01, NMI: 0.01	 (j) $k_p = 3$ , PA: 34.42, NMI: 0.64	 (k) $k_p = 2$ , PA: 10.01, NMI: 0.01	 (l) $k_p = 5$ , PA: 34.55, NMI: 0.63	 (m) $k_p = 0$ , PA: 10.47, NMI: 0.01	 (n) $k_p = 5$ , PA: 34.42, NMI: 0.62
( $k = 10$ ) CIFAR 10	 (o) $k_p = 6$ , PA: 54.12, NMI: 0.49	 (p) $k_p = 0$ , PA: 10.13, NMI: 0.006	 (q) $k_p = 4$ , PA: 18.25, NMI: 0.07	 (r) $k_p = 2$ , PA: 10.13, NMI: 0.006	 (s) $k_p = 4$ , PA: 17.32, NMI: 0.27	 (t) $k_p = 0$ , PA: 11.56, NMI: 0.01	 (u) $k_p = 2$ , PA: 10.31, NMI: 0.02
( $k = 10$ ) INTEL	 (v) $k_p = 6$ , PA: 57.32, NMI: 0.44	 (w) $k_p = 0$ , PA: 15.21, NMI: 0.009	 (x) $k_p = 3$ , PA: 31.27, NMI: 0.20	 (y) $k_p = 2$ , PA: 17.13, NMI: 0.006	 (z) $k_p = 0$ , PA: 17.85, NMI: 0.007	 (aa) $k_p = 0$ , PA: 19.42, NMI: 0.006	 (ab) $k_p = 1$ , PA: 19.78, NMI: 0.009
( $k = 6$ )							

Fig. 3: Comparison of DeepVAT with iVAT, FensivAT and KernelVAT

namely KernelVAT [8] and FensivAT [7]. In KernelVAT, radial basis function (RBF) kernel is used, with the precision parameter ( $\gamma$ ) set to 0.05. In FensivAT, the downspace (reduced) dimension for random projection is chosen 100 when FensivAT is applied to raw flattened image or a 2048-dimensional SimCLR embedding. For a fair comparison, we also compare iVAT, KernelVAT and FensivAT on t-SNE reduce dimensions to show that DeepVAT doesn't get benefit only from t-SNE. When the input data is t-SNE-reduced to 2 dimensions, the downspace dimension in FensivAT is set to 2.

We compare DeepVAT with the following methods:

- **iVAT**: iVAT is applied on a small MMRS subset of raw flattened images. We denote the resulting RDI as  $I(\mathbf{D}_V)$ .
- **iVAT + tSNE**: We flattened every image in the dataset and reduced their dimensionality to 2 using t-SNE. Then, we sampled a small subset of the data using MMRS and applied iVAT on that subset. We denote the RDI as  $I(\mathbf{D}_{V-t-SNE})$ .
- **FensivAT**: FensivAT is applied on a small MMRS subset of the raw flattened images. The resulting RDI is denoted as  $I(\mathbf{D}_F)$ .
- **FensivAT + t-SNE**: We flattened every image in the

dataset and reduced their dimensionality to 2 using t-SNE. Then, we sampled a small subset of the data using MMRS and applied FensivAT on this subset. The resulting RDI is denoted as  $I(\mathbf{D}_{F-t-SNE})$ .

- **KernelVAT**: KernelVAT is applied on a small MMRS subset of the raw flattened images. The resulting RDI is denoted as  $I(\mathbf{D}_K)$ .
- **KernelVAT + t-SNE**: We flattened every image in the dataset and reduced their dimensionality to 2 using t-SNE. We then sampled a small subset of the data using MMRS and applied KernelVAT on this subset. The resulting RDI is denoted as  $I(\mathbf{D}_{K-t-SNE})$ .

Table I shows the comparison of DeepVAT with all six models with corresponding iVAT images based on the estimated number of clusters ( $k_p$ ), PA and NMI. The first column shows the dataset and true number of labeled subsets ( $k$ ) in it, and other six columns shows iVAT RDI, estimated number of clusters ( $k_p$ ), PA and NMI for each method. We can see that DeepVAT method generates much clearer and sharper dark blocks compared to the simple iVAT, KernelVAT and FensivAT models. Consequently, the number of dark blocks generated by DeepVAT ( $k_p$ ) is close to the original number

of classes ( $k$ ) in the dataset, making it the most accurate in estimating the potential number of clusters compared to other algorithms. Applying iVAT directly to the high-dimensional embedding yields a blurry image  $I(\mathbf{D}_V)$ , and poor quantitative results. However, when t-SNE is applied to the raw data, it gives better quality RDI,  $I(\mathbf{D}_{V_{t-SNE}})$ , compared to the  $I(\mathbf{D}_V)$ . Surprisingly, KernelVAT fails miserably when applied directly to the flattened raw data. These results suggest that our approach produces more visually appealing and informative representations of the data. As a result, DeepVAT also outperforms all the six competitive models in terms of PA and NMI scores.

The success of DeepVAT can be attributed to the use of SimCLR and t-SNE. SimCLR is effective at generating a robust representation of the dataset by leveraging non-linear functions, such as deep CNN encoders and projection heads, to approximate its intrinsic dimensionality. By applying t-SNE on the representation produced by SimCLR, we obtain a better low-dimensional embedding, as SimCLR is better equipped to detect highly varying manifolds than t-SNE alone.

## V. CONCLUSIONS AND FUTURE WORK

This article proposes a deep, self-supervised learning based VAT framework, DeepVAT, for cluster structure assessment in high-dimensional data. The self-supervised learning method SimCLR significantly improved the performance of iVAT both qualitatively and quantitatively. Our experimental results suggest that when t-SNE is used as dimensionality reduction on top of SimCLR embeddings, the iVAT yields much sharper RDI, thus more accurate estimate of the number of clusters. This is because SimCLR can capture the intrinsic dimensionality of image datasets which helped t-SNE in generating a good low dimensional representation. Based on our numerical experiments on four high-dimensional, image datasets, we have also shown that DeepVAT significantly outperformed other VAT family methods FensIVAT and KernelVAT based on clustering partition accuracy and NMI. We believe that deploying more deep learning based models like deep metric learning and semi-supervised, which have partial access to labels can further improve the iVAT image for complex datasets.

At present, the training time for major self-supervised contrastive learning models is quite extensive. As part of our future work, we aim to focus on reducing the training time required for such models. Our objective is to develop methods that can generate high-quality iVAT images using self-supervised contrastive learning models in significantly less time.

## REFERENCES

- [1] A. K. Jain, R. C. Dubes *et al.*, *Algorithms for clustering data*. Prentice hall Englewood Cliffs, 1988, vol. 6.
- [2] B. S. Everitt, *Graphical techniques for multivariate data*. North-Holland, 1978.
- [3] W. S. Cleveland, *Visualizing data*. Hobart Press, 1993.
- [4] J. C. Bezdek and R. J. Hathaway, "Vat: A tool for visual assessment of (cluster) tendency," in *Proceedings of the 2002 International Joint Conference on Neural Networks. IJCNN'02 (Cat. No. 02CH37290)*, vol. 3. IEEE, 2002, pp. 2225–2230.
- [5] R. C. Prim, "Shortest connection networks and some generalizations," *The Bell System Technical Journal*, vol. 36, no. 6, pp. 1389–1401, 1957.
- [6] T. C. Havens and J. C. Bezdek, "An efficient formulation of the improved visual assessment of cluster tendency (ivat) algorithm," *IEEE Transactions on Knowledge and Data Engineering*, vol. 24, no. 5, pp. 813–822, 2011.
- [7] P. Rathore, D. Kumar, J. C. Bezdek, S. Rajasegarar, and M. Palaniswami, "A rapid hybrid clustering algorithm for large volumes of high dimensional data," *IEEE Transactions on Knowledge and Data Engineering*, vol. 31, no. 4, pp. 641–654, 2018.
- [8] B. Zhang, Y. Zhu, S. Rajasegarar, G. Li, and G. Liu, "Kernel-based ivat with adaptive cluster extraction," 2022.
- [9] T. C. Havens, J. C. Bezdek, and M. Palaniswami, "Scalable single linkage hierarchical clustering for big data," in *IEEE Eighth International Conference on Intelligent Sensors, Sensor Networks and Information Processing*. IEEE, 2013, pp. 396–401.
- [10] L. Wang, X. Geng, J. Bezdek, C. Leckie, and R. Kotagiri, "Specvat: Enhanced visual cluster analysis," in *2008 eighth IEEE international conference on data mining*. IEEE, 2008, pp. 638–647.
- [11] R. J. Hathaway, J. C. Bezdek, and J. M. Huband, "Scalable visual assessment of cluster tendency for large data sets," *Pattern Recognition*, vol. 39, no. 7, pp. 1315–1324, 2006.
- [12] M. E. Johnson, L. M. Moore, and D. Ylvisaker, "Minimax and maximin distance designs," *Journal of statistical planning and inference*, vol. 26, no. 2, pp. 131–148, 1990.
- [13] T. Chen, S. Kornblith, M. Norouzi, and G. Hinton, "A simple framework for contrastive learning of visual representations," in *International conference on machine learning*. PMLR, 2020, pp. 1597–1607.
- [14] J. Zbontar, L. Jing, I. Misra, Y. LeCun, and S. Deny, "Barlow twins: Self-supervised learning via redundancy reduction," in *International Conference on Machine Learning*. PMLR, 2021, pp. 12 310–12 320.
- [15] S. Avidan, G. Brostow, M. Cissé, G. M. Farinella, and T. Hassner, *Computer Vision—ECCV 2022: 17th European Conference, Tel Aviv, Israel, October 23–27, 2022, Proceedings, Part XX*. Springer Nature, 2022, vol. 13680.
- [16] X. Chen and K. He, "Exploring simple siamese representation learning," in *Proceedings of the IEEE/CVF conference on computer vision and pattern recognition*, 2021, pp. 15 750–15 758.
- [17] J.-B. Grill, F. Strub, F. Altché, C. Tallec, P. Richemond, E. Buchatskaya, C. Doersch, B. Avila Pires, Z. Guo, M. Gheshlaghi Azar *et al.*, "Bootstrap your own latent—a new approach to self-supervised learning," *Advances in neural information processing systems*, vol. 33, pp. 21 271–21 284, 2020.
- [18] A. v. d. Oord, Y. Li, and O. Vinyals, "Representation learning with contrastive predictive coding," *arXiv preprint arXiv:1807.03748*, 2018.
- [19] L. Van der Maaten and G. Hinton, "Visualizing data using t-sne," *Journal of machine learning research*, vol. 9, no. 11, 2008.
- [20] Y. LeCun, C. Cortes, and C. J. Burges, "Mnist handwritten digit database," *ATT Labs [Online]*. Available: <http://yann.lecun.com/exdb/mnist>, 2010.
- [21] H. Xiao, K. Rasul, and R. Vollgraf, "Fashion-mnist: a novel image dataset for benchmarking machine learning algorithms," *arXiv preprint arXiv:1708.07747*, 2017.
- [22] A. Krizhevsky, "Cifar-10 (canadian institute for advanced research)," <https://www.cs.toronto.edu/~kriz/cifar.html>, 2009.
- [23] I. Corporation, "Intel image classification," <https://software.intel.com/content/www/us/en/develop/articles/image-classification-using-convolutional-neural-networks-on-intel-architecture.html>, 2016.
- [24] Y. You, I. Gitman, and B. Ginsburg, "Large batch training of convolutional networks," *arXiv preprint arXiv:1708.03888*, 2017.